JOURNAL OF APPLIED ELECTROCHEMISTRY **28** (1998) 593–600

Electrooxidation of 1024 mild steel in slightly alkaline phosphate and bicarbonate solutions

S. SIMARD, H. MÉNARD

Département de Chimie, Université de Sherbrooke, Sherbrooke, Québec, Canada J1K 2R1

L. BROSSARD

Institut de recherche d'Hydro-Québec (IREQ), 1800 boul. Lionel-Boulet, Varennes, Québec, Canada J3X 1S1

Received 3 March 1997; revised 8 September 1997

The electrochemical behaviour of 1024 mild steel electrodes was investigated in the presence of 0.05–0.5 M disodium phosphate aqueous solution, in the pH range 8.4 to 9.7 and from 5 to 50 °C. Bicarbonate solutions were also considered for comparison. Voltammograms were obtained with a rotating gold ring steel disc electrode, and the effects of the phosphate concentration, pH, electrode rotation speed, anodic potential limit and temperature were considered. For potential sweeps in the anodic direction in phosphate solutions, the voltammograms display an oxidation peak current at low potentials and a passivity region at higher potentials. The rate-determining step of the oxidation peak current was also investigated. The oxidation current in the passivity region is virtually independent of the applied potential, temperature, pH and phosphate concentration.

Keywords: *electrooxidation*, *1024 mild steel*, *localized attack*, *phosphate solution*, *bicarbonate solution*

1. Introduction

Bicarbonate, phosphate and chloride ions may be found in natural water where their ability to form soluble complexes and their buffering capacity may affect the corrosion or the protection of mild steel. Each ionic species has a different effect on the electrochemical behaviour of mild steel depending on the ambient conditions, especially the ion concentration, potential, pH range and temperature. The potentiodynamic behaviour of 1024 mild steel was investigated in relation to the effect of dissolved bicarbonate/carbonate both alone [1] and in the presence of chloride ions [2]. The potentiodynamic curve is characterized by three potential regions in aqueous sodium bicarbonate solutions at pH 8.9 and at room temperature. An active dissolution region is observed at low potentials, while at more anodic potentials, a passive region followed by a transpassive region is noted. The diffusion of the ionic species in the solution near the electrode surface plays a key role in limiting the dissolution process in both the active and transpassive regions. It is suggested that the formation of $FeHCO_3^+$ is involved in the dissolution region.

Passive film stability under experimental conditions similar to those of [1] (except for the presence of chloride ions) was further investigated [2]. The presence of sodium bicarbonate in solution has an inhibitive effect on the localized attack induced by chloride anions. The passive film breakdown is dependent on the preanodization potential. All the experiments for the two references given above were carried out at 25 °C.

Phosphate is considered to be an inorganic anodic corrosion inhibitor in aqueous solutions. It is commonly linked to mild steel due to the conversion protective coating obtained by the phosphating in acidic media. Industrially known conversion coatings were still recently under investigation [3]. Phosphate is also a complex buffer characterized by a three-step dissociation. The effect of each species generated by these dissociations has not been extensively studied as far as the electrochemical behaviour of mild steel is concerned. It was demonstrated that the presence of such buffer anions in bicarbonate media can have a major impact on the electrochemical behaviour of mild steel [1].

However, many studies have focussed on determining the composition, mechanism and/or kinetics of passive film growth [4]. The composition of the passive film in deaerated phosphate aqueous media has been discussed and most of the papers consider the presence of γ-Fe_2O_3 [5–11]. Layered passive films have also been taken into consideration [6, 9, 12]. The presence of films containing phosphate [3, 10, 12–17] or some phosphate groups bonded to the oxide film were reported under various experimental conditions [18]. The effect of the presence of phosphate in the film was also discussed [14, 19] and the specific composition of the iron phosphates involved was also reported as an important factor in corrosion inhibition. The inhibitive effect of phosphate was related to the solution pH [20]. Moreover, despite the fact that

0021-891X

the passive films in solutions containing phosphate have been investigated extensively, little attention has been paid to the breakdown of such films [4, 9, 21, 22]. HPO_4^{2-} is reported as the most effective inhibitive anion compared to citrate, benzoate, carbonate and acetate [21].

The term 'inhibitor' ions is used to indicate that an ion contributes to preventing greater metal oxidation than in the absence of this particular ion. Such ions can be considered as inhibitors only in a limited potential area. For example, the presence of bicarbonate/carbonate ions is beneficial in the passive region since ionic species play a key role in the growth of a protective passive film which acts as a protector against the localized attack induced by the presence of aggressive anions such as chloride ions [2]. On the other hand, the presence of carbonate/bicarbonate is a determining element in the active electrodissolution region [1, 23] and in the transpassive region [1]. This paper focuses on the electrodissolution of 1024 mild steel in slightly alkaline phosphate solution with special emphasis on the effect of the solution's composition. The composition of the phosphate solutions is largely pH-dependent and it is of paramount importance to determine the specific role of each ionic species generated by the three-step dissociation of the phosphate. A comparative analysis of bicarbonate and phosphate solutions is also used to investigate the effect of the nature of the ionic species on the electrooxidation process and on the localized attack induced by the presence of chloride ions.

2. Experimental details

The experiments were carried out with a rotating disc electrode or a rotating ring disc electrode. In both cases, the disc electrode was a mild steel (1024) disc whose composition is given elsewhere [1].

The disc electrode had a surface area of 0.126 cm^2. The rotating gold ring-steel disc electrode had a steel disc diameter of 5 mm while the gold ring had an inner diameter of 5.15 mm and an outer diameter of 7.2 mm ($N = 0.4715$ for calculated collection efficiency) [24]. The disc and ring-disc electrodes were set in a Kel-F holder. The auxiliary electrode was a platinized platinum grid separated from the main compartment by a Nafion® membrane. The reference electrode was a saturated calomel electrode (SCE) connected to the cell by a bridge and a Luggin capillary. All the potentials quoted below are referenced to this electrode. Since the presence of aqueous Fe(II) in the solution can eventually influence the nature of the oxide film [25], the volume of the electrochemical cell used was at least of 0.55 dm^3, so that the concentration of dissolved iron in the bulk of the solution could be neglected.

Aqueous solutions were prepared with BDH Assured® or Anachemia® analytical reactant grade chemicals using deionized water. The pH of the solutions was adjusted with a NaOH solution. The solutions were deaerated using high-purity nitrogen bubbling before and during the experiments. The electrode surfaces were ground with 600, 3/0 emery papers and mechanically polished with 1.0 and 0.05 μm alumina suspensions before each immersion.

The measurements on the rotating disc electrode were performed with a PAR 273A potentiostat controlled by a computer, using M270 electrochemical software. The measurements with the rotating ring disc electrode were taken with a Pine Instrument model AFRDE4 bipotentiostat and the output signal was converted from analog to digital and recorded on an IBM-compatible computer. A Pine Instrument analytical rotator was used for the electrodes.

3. Results

3.1. *Electrochemical behaviour*

Figure 1 shows the potentiodynamic curve ($dE/dt = 5$ mV s^{-1}) for a 1024 mild steel disc electrode rotated at 1000 rpm in 0.1 M Na_2HPO_4 solution (pH 8.9). The curve displays a large oxidation current peak located at −0.65 V, is followed by a passive region extending over 1.4 V (i.e. from −0.5 to 0.9 V). The oxidation current is close to 0.02 mA cm^{-2} in the passive region. The stabilization of the potentiodynamic traces is observed after the first complete potential cycle under the experimental conditions of Fig. 1. The potentiodynamic curve during the return sweep is characterized by a small reduction current peak located at −0.6 V.

The height of the anodic peak current (J_p) is dependent on the rotation speed (ω) of the mild steel disc electrode (Fig. 2), with the plot of J_p^{-1} against $\omega^{-1/2}$ giving a linear relationship with $J_p^{-1} \neq 0$ for $\omega^{-1/2} = 0$. One notes the presence of a shoulder on the descending part of the oxidation peak (peak I) as the rotation speed is low, and a maximum peak close to −0.45 V (peak II) for a stationary electrode. The electrooxidation rate close to −0.45 V is virtually in-

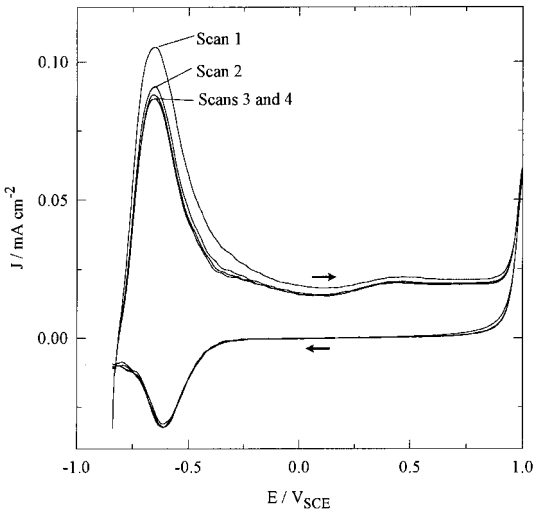

Fig. 1. Cyclic voltammograms for a 1024 mild steel electrode rotated at 1000 rpm in 0.1 M Na_2HPO_4 at pH 8.9. $dE/dt = 0.005$ V s^{-1}.

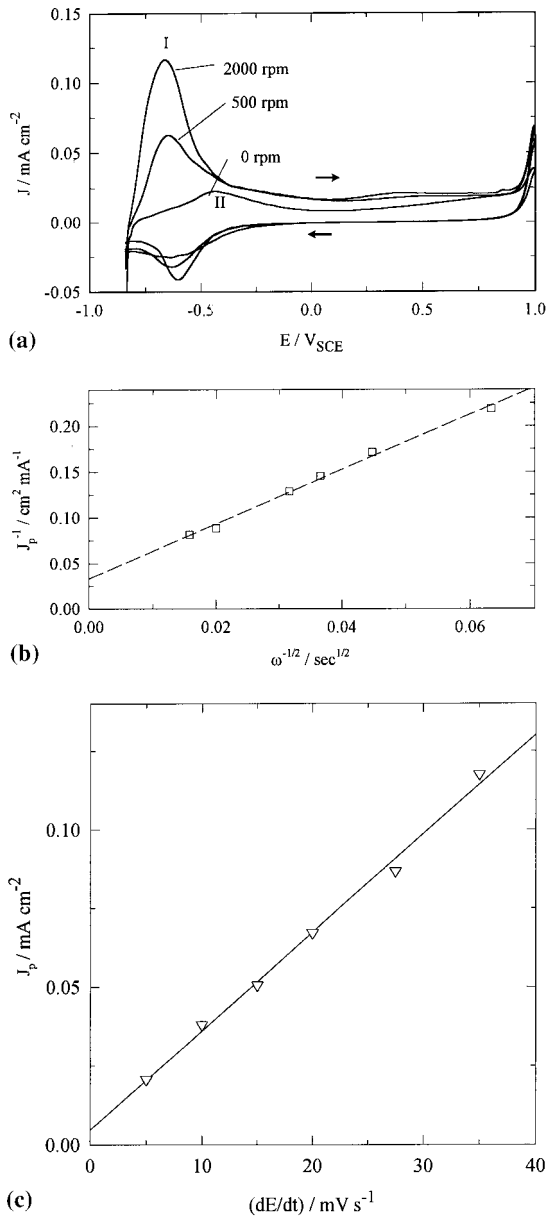

Fig. 2 (a) Cyclic voltammograms for a 1024 mild steel electrode for various ω in 0.1 M Na_2HPO_4 at pH 8.9. $dE/dt = 0.005$ V s^{-1}; (b) $1/j_p$ against $\omega^{-1/2}$ for a 1024 mild steel disc; (c) j_p against v for the peak II ($\omega = 0$ s^{-1}), i.e. a stationary electrode.

dependent of ω. Moreover, peak current II is related to the scan rate (v) using the linear relationship J_p against v (Fig. 2(c)).

The current at the rotating ring electrode was recorded to allow the detection of Fe(II) soluble species generated at the disc electrode during mild steel electrodissolution. The potential at the ring was maintained constant at 0.4 V to further oxidize Fe(II) soluble species. An oxidation current peak is detected at the ring electrode simultaneously with the oxidation current peak at the disc electrode (Fig. 3). In the passivity region, the current at the ring electrodes is close to zero.

The stabilized potentiodynamic curves obtained in 0.1 M $NaHCO_3$ and 0.1 M Na_2HPO_4 aqueous solution of pH 8.9 for rotating disc electrodes at $\omega = 1000$ rpm are illustrated on Fig. 4. It is noted

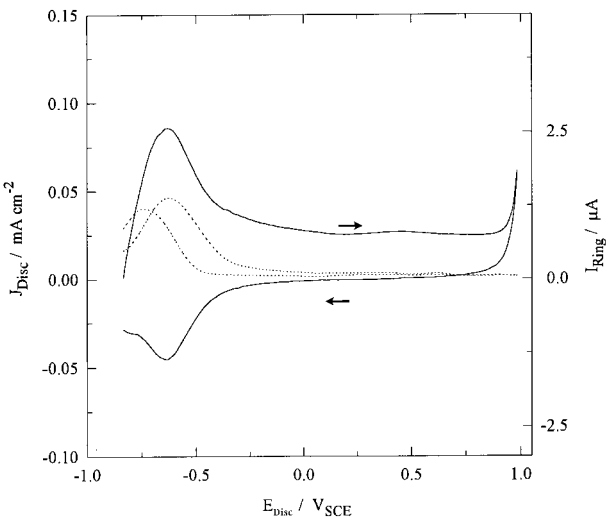

Fig. 3. Current at gold ring electrode during potential sweep of the mild steel disc electrode. Electrode rotation speed = 1000 rpm. Solution: 0.1 M Na_2HPO_4 (pH 8.9). The disc scan rate was $dE/dt = 0.005$ V s^{-1} and $E_{ring} = 0.4$ V. Key: (——) disc, (. . . . . .) ring.

that the height of the anodic current peak located at around −0.65 V is five times smaller in the case of phosphate than bicarbonate solution, with the maximum current peak being 20 mV more cathodic for the latter solution. In the passive region, the small oxidation current is practically the same for both solutions. As the potential becomes sufficiently anodic, the large current density increase corresponds to ~0.85 V for 0.1 M $NaHCO_3$ solution compared to ~0.95 V for Na_2HPO_4 solution. Furthermore, the cathodic maximum peak current noticed during the return sweep has a potential that is ~0.1 V more anodic for 0.1 M Na_2HPO_4 than for 0.1 M $NaHCO_3$.

The potentiodynamic curves recorded for mild steel in 0.075 to 0.5 M Na_2HPO_4 solutions (Fig. 5) show that the higher the concentration in dissolved Na_2HPO_4, the higher the oxidation peaks (J_p) (Fig. 6(a)). A linear relationship is observed as J_p is plotted against $[Na_2HPO_4]^{1/2}$ (Fig. 6(b)).

The oxidation current in the passive region is virtually constant, ranging from 0.075 to 0.5 M Na_2HPO_4. A broad reduction current peak located at −0.63 V is observed for 0.075 M Na_2HPO_4. The

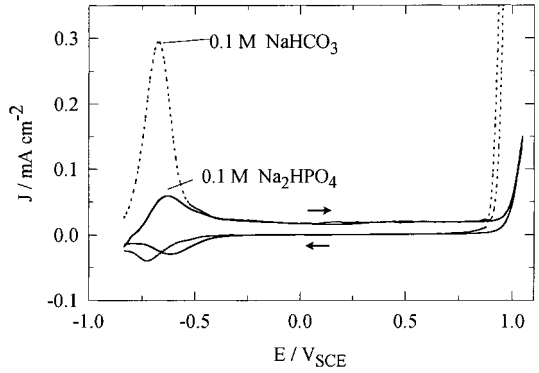

Fig. 4. Cyclic voltammograms for a 1024 mild steel electrode rotated at 1000 rpm in 0.1 M Na_2HPO_4 and $NaHCO_3$ at pH 8.9. $dE/dt = 0.005$ V s^{-1}.

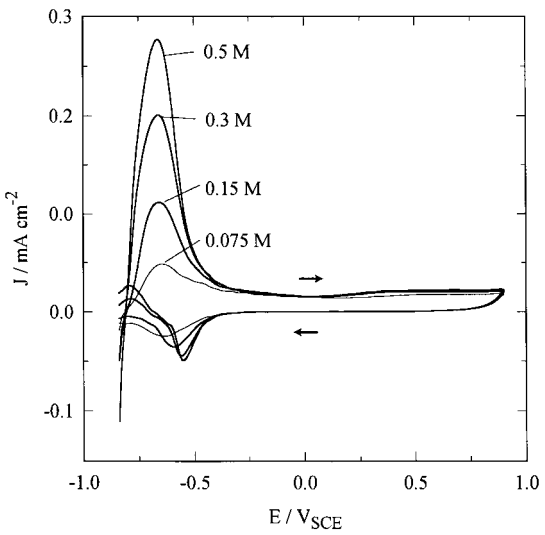

Fig. 5. Effect of phosphate concentration on the potentiodynamic curves for a 1024 mild steel electrode, $\omega = 1000$ rpm, pH 8.9 and $dE/dt = 0.005$ V s^{-1}.

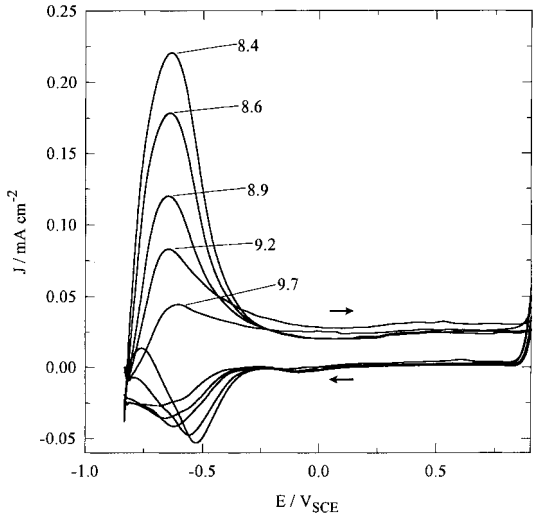

Fig. 7. Potentiodynamic traces for a 1024 mild steel disc electrode rotated at 1000 rpm in 0.1 M Na_2HPO_4 at various pH values. $dE/dt = 0.005$ V s^{-1}.

reduction peak becomes sharper and shifts in the anodic direction as the Na_2HPO_4 concentration is increased, i.e. the maximum peak current is located at −0.55 V for $[Na_2HPO_4] = 0.5$ M.

The pH effect on the potentiodynamic behaviour of mild steel was investigated in 0.1 M Na_2HPO_4 solutions, with the pH ranging from 8.4 to 9.7 (Fig. 7). The anodic oxidation peak current at around −0.65 V is considerably larger when the pH is decreased, and the current density in the passive region is almost independent of the pH. For the potential sweep in the cathodic direction, the smaller the pH, the smaller the reduction peak and the more anodic its location. A reactivation (oxidation) process of the electrode is observed for the curve at pH 8.4.

3.2. *Reversal of the potential sweep*

Voltammograms with an increase in the anodic potential sweep limit ($E_{1.a.}$) greater than −0.4 V for a 1024 mild steel electrode rotated at 1000 rpm and with $dE/dt = 5$ mV s^{-1} in 0.1 M Na_2HPO_4 solution are presented in Fig. 8. The more anodic $E_{1.a.}$, the higher the reduction current peak (−0.6 V) on the cathodic section of the potential scan, with the reduction peak being followed by an oxidation current for $E_{1.a.}$ below 0.4 V. A cathodic peak only is observed for $E_{1.a.}$ of 0.4 V.

Further information about the oxide film is obtained from the galvanostatic reduction experiments. A current against time curve of a rotated (1000 rpm) mild steel disc electrode preanodized at 0.8 V during 3 h in 0.1 M Na_2HPO_4 is presented in Fig. 9. Immediately after oxidation, a cathodic current of 800 nA cm^{-2} was applied to the electrode and the potential was measured during the reduction process. It is shown that the transient potential starts at about 0.35 V and decays rapidly over time to reach poten-

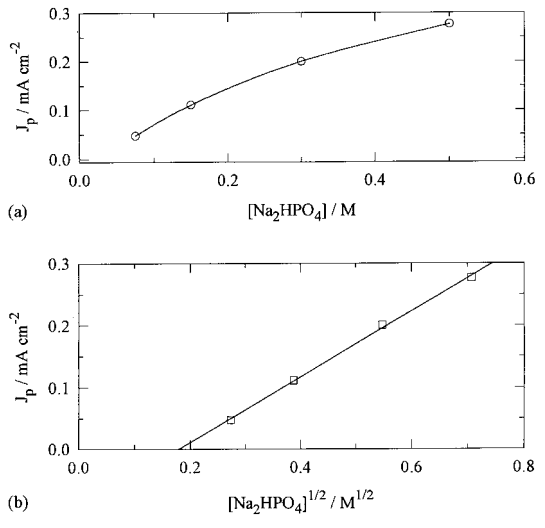

Fig. 6. Plots involving J_p obtained from Fig. 5 against Na_2HPO_4.

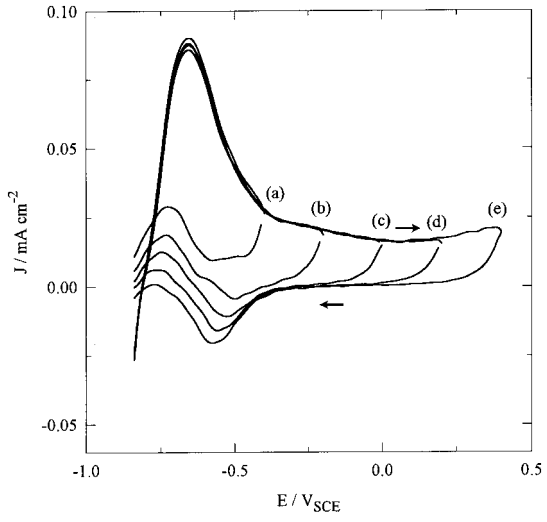

Fig. 8. Potentiodynamic curves for different positive potential limits: (a) −0.4, (b) −0.2, (c) 0.0, (d) 0.2 and (e) 0.4 V. $\omega = 1000$ rpm. $dE/dt = 0.005$ V s^{-1}. Solution: 0.1 M Na_2HPO_4 (pH 8.9).

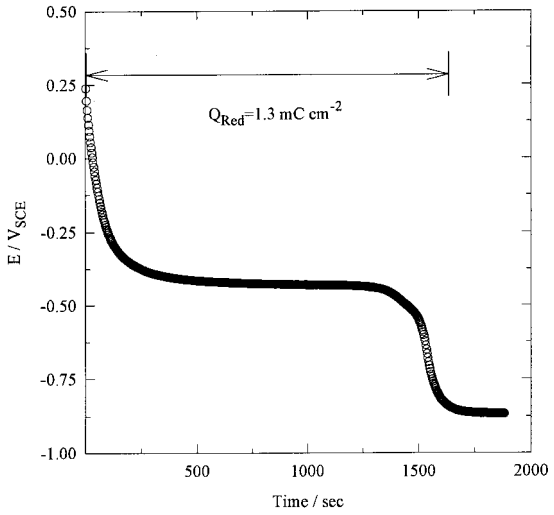

Fig. 9. Chronopotentiometric curves recorded with a reduction current of 800 nA cm^{-2} after preanodization. 1024 mild steel disc electrode in 0.1 M Na_2HPO_4. ω = 1000 rpm. pH 8.9. Preanodization at 0.8 V for 3 h ($Q \simeq 10$ mC cm^{-2}).

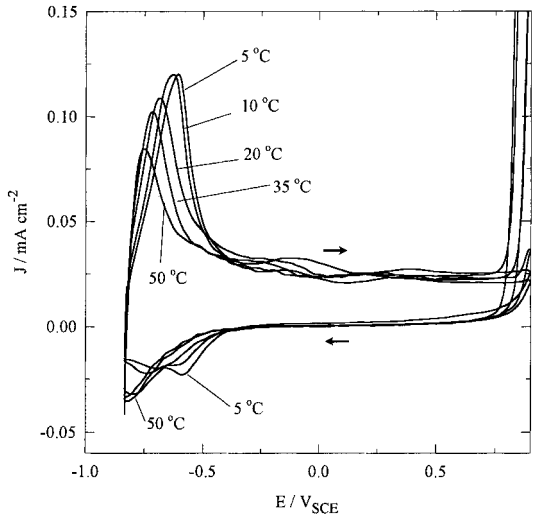

Fig. 11. Cyclic voltammograms for a 1024 mild steel electrode rotated at 1000 rpm in 0.1 M $NaHCO_3$ at pH 8.9 at various temperatures. dE/dt = 0.005 V s^{-1}.

tial arrest at about −0.4 V. The total duration of the film reduction was about 1600 s, which corresponds to a reduction charge of about 1.3 mC cm^{-2}.

3.3. *Effect of temperature in $NaHCO_3$ and Na_2HPO_4 solutions*

The effect of temperature on the potentiodynamic curves for the phosphate (Fig. 10) and bicarbonate (Fig. 11) buffer was investigated. The following is deduced from the potentiodynamic curves of Fig. 10 for a phosphate buffer at a temperature ranging from 5 to 50 °C: (i) above 20 °C, the oxidation peak current (−0.65 V) in the phosphate buffer is only slightly temperature-dependent; for curves obtained at 35 and 50 °C, the higher the temperature, the lower the peak current; (ii) the presence of a shoulder at potentials more anodic than the peak current is marginal at 35 °C but clearly distinguishable at 50 °C; (iii) the current in the passive region is temperature-independent from 5 to 35 °C, the current being larger at 50 °C. The potentiodynamic traces during the return sweep remain unchanged from 5 to 35 °C.

The situation regarding the potentiodynamic behaviour of mild steel in bicarbonate solutions is slightly different (Fig. 11): (i) the higher the temperature, the lower the anodic peak current and the more negative the location of this peak current. In the passive region, the oxidation current is virtually unchanged from 5 to 35 °C; (ii) the curves display two reduction peaks during the return sweep: the first one located at about −0.590 V, the second one at about −0.790 V. The first reduction peak current is negligible or absent from 20 to 50 °C, with the effect of the temperature going in the opposite direction for the first and the second reduction peak.

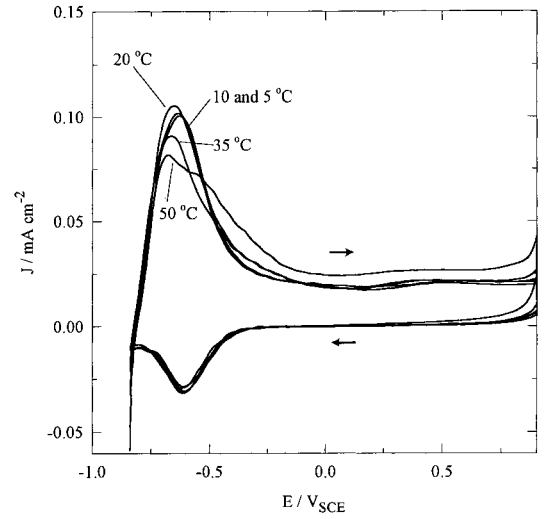

Fig. 10. Cyclic voltammograms for a 1024 mild steel electrode rotated at 1000 rpm in 0.1 M Na_2HPO_4 at pH 8.9 at various temperatures. dE/dt = 0.005 V s^{-1}.

3.4. *Localized attack induced by Cl^-*

In a first set of experiments, the localized attack induced by the presence of Cl^- ions was characterized for bicarbonate and phosphate aqueous solutions at 20 °C. The electrode potential was swept (dE/dt = 1 mV s^{-1}) in the anodic direction from −0.835 V in 0.1 M $NaHCO_3$ + 0.15 M NaCl (Fig. 12(a)) and 0.1 M Na_2HPO_4 + 0.15 M NaCl (Fig. 12(b)) solution at pH 9. For the bicarbonate solution, the film breakdown occurs at a given potential value and is characterized by a rapid current increase.

For the phosphate solution, the film breakdown potential may vary largely from one experiment to another, with the experimental conditions being the same. Moreover, some current oscillations may be observed before film breakdown.

SEM pictures of localized attack sites on mild steel are shown in Fig. 13(a) for a bicarbonate buffer and in Fig. 13(b) for a phosphate buffer. The precipitate

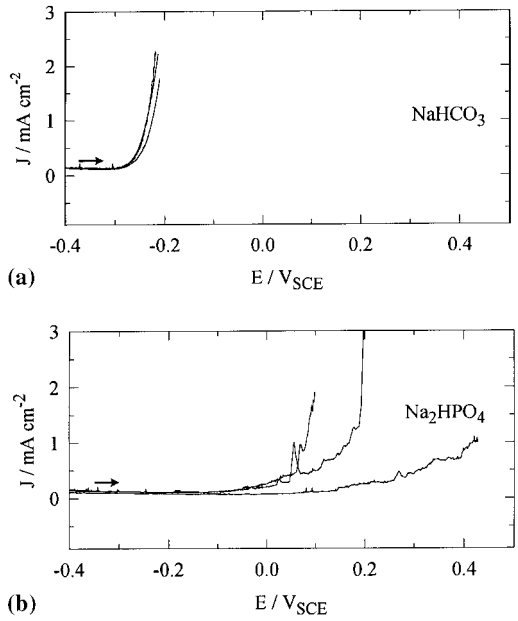

Fig. 12. Potentiodynamic curves for a 1024 mild steel electrode rotated at 1000 rpm in 0.15 M NaCl at pH 8.9 and (a) 0.1 M $NaHCO_3$, (b) 0.1 M Na_2HPO_4.

covering the pit has a different morphology depending on the composition of the solution. The precipitate is less porous when formed in the phosphate solution compared to a bicarbonate solution. The solid formed in the presence of the phosphate buffer presents some cracks on its surface and a long tail.

The temperature effect on the breakdown potential (Fig. 14) shows that the breakdown potential is temperature-dependent for a steel-disc electrode (ω = 1000 rpm) in 0.1 M $NaHCO_3$ bicarbonate solution containing 0.15 M NaCl. It is noted that the breakdown potential is located at about −0.175 V at 5 °C and shifts in the cathodic potential direction when the temperature is raised. The breakdown potential is practically constant from 35 to 50 °C, with its minimum value being close to −0.280 V.

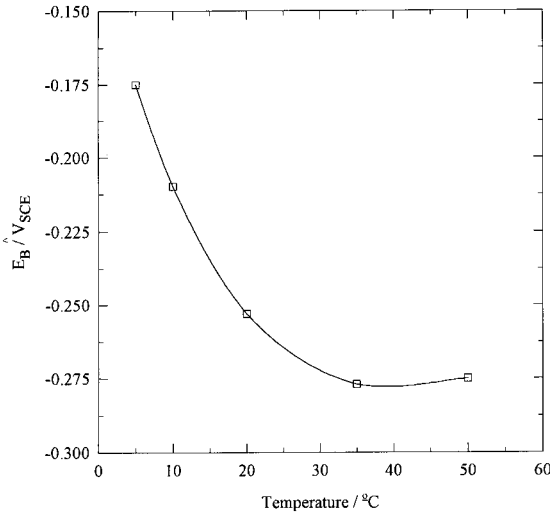

Fig. 14. Breakdown potentials measured at various solution temperatures. Solution: 0.1 M $NaHCO_3$ and 0.15 M Cl^-. ω = 1000 rpm.

For the phosphate buffer, it was not possible to determine the effect of the temperature on the film breakdown since the latter is not sufficiently reproducible.

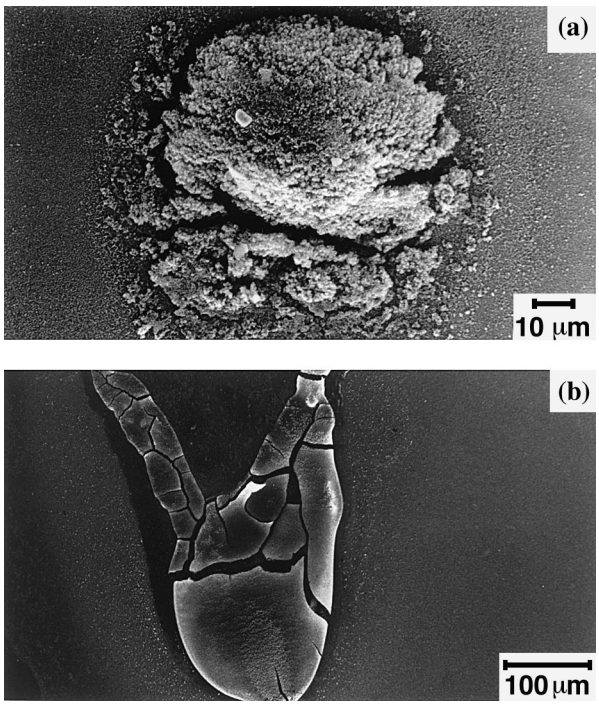

Fig. 13. Scanning electron microscopy picture obtained for an electrode after a potentiodynamic scan under the same experimental conditions as in Fig. 12.

4. Discussion

4.1. *Active dissolution region*

The anodic dissolution peak located at −0.6 V on the potentiodynamic traces in 0.1 M Na_2HPO_4 (Fig. 1) is related to the active dissolution of mild steel. The results obtained with the RRDE electrode (Fig. 3) indicate that mild steel most likely leads to the electrogeneration of Fe(II) soluble species or a complex with Fe(II), with the amount of solid oxide accumulated at the surface being negligible.

It is deduced from the dependence of the peak current on both the disc electrode rotation speed (Fig. 2) and the phosphate concentration (Fig. 5) that phosphate ions are involved in the electrodissolution process. The linear relationship of J_p^{-1} against $\omega^{-1/2}$ indicates that the diffusion of ionic species in the solution plays a key role in limiting the oxidation process. The catalysis of the electrodissolution through the formation of soluble complexes may be considered.

Since phosphate is a three-valent ion and its dissociation involves three successive steps, the formation of complexes may involve PO_4^{3-}, HPO_4^{2-} and $H_2PO_4^-$ species. It is possible to change the ratio of each species by varying the solution pH. Figure 15(a) shows the molar fraction (α) of each phosphate species against the solution pH. The concentration of

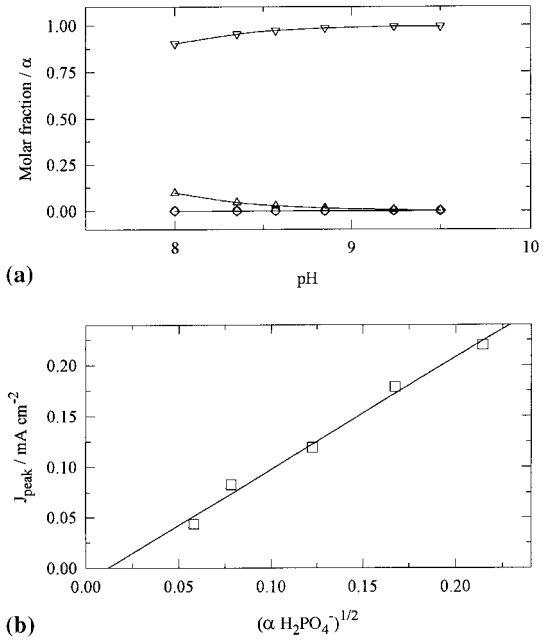

Fig. 15. (a) Calculated composition of a phosphate solution at various pH. Fraction: (○) H_3PO_4, (△) $H_2PO_4^-$, (▽) HPO_4^{2-}, (◇) PO_4^{3-}. (b) Correlated curve of the peak current obtained in Fig. 7 and the molar fraction from Fig. 15(a).

each species is proportional to its molar fraction at a given pH. Since the peak current decreases for increasing pH, the involvement of $H_2PO_4^-$ species is considered to be the rate-determining-step of the electrooxidation process. This is supported by the linear relationship of J_p against $(\alpha_{H_2PO_4^-})^{1/2}$ (Fig. 15(b)) and of J_p against $[Na_2HPO_4]^{1/2}$ given in Fig. 6. From the above considerations, it is deduced that $2Fe + H_2PO_4^- \rightarrow [Fe_2, H_2PO_4^-] + ne^-$. $[Fe_2, H_2PO_4^-]$ is an iron/phosphate complex, with its nature still to be determined. The rate-determining-step in the active dissolution region is ascribed to the diffusion of the iron/phosphate complex from the electrode surface to the solution.

The active dissolution process in phosphate solution is not significantly altered from 5 to 20 °C. However, the higher the temperature above 20 °C, the lower the dissolution rate, that is, the passivation process seems to arise at more cathodic potentials while the cathodic side of the electrodissolution peak (peak I) remains unchanged as T is increased. This phenomenon is most likely linked to a shift in the cathodic direction of the surface reaction current peak (peak II) involved in the beginning of the passivation.

For the bicarbonate solution, both processes, that is, active dissolution and passivation, are shifted in the cathodic direction at higher temperature. In this case, the temperature has an effect in both the active dissolution and passivation processes.

4.2. *Passive region*

In phosphate solution, the mild steel electrodissolution process is slowed down by the formation of a passive film, with the beginning of the passivation being characterized by the presence of peak II, which is evidenced under stationary conditions (Fig. 2(a)); its height is directly proportional to the scan rate (i.e. $J_p \propto v$) and is virtually independent of ω. Consequently, the rate-determining step in the region of peak II is linked to a surface reaction.

The potentiodynamic curves for a rotating disc electrode shows that the film becomes more stable during the return sweep as the anodic potential limit is increased. The stable passive layer is most likely formed in the region of 0.4 V since no reactivation is noticed on the cathodic section of the potentiodynamic curve. At high potentials, the formation of γ-Fe_2O_3 has been proposed by many authors [1, 5–11]. At lower potentials, the presence of Fe_3O_4 is suggested [10, 12]. In deaerated slightly alkaline solutions, the presence of iron phosphate was not commonly reported. It can be suggested that the composition of the passive film is similar to the one formed in bicarbonate solutions [1].

The cathodic current peak linked to the reduction of the passive film is catalysed by the phosphate in solution because the potential necessary for the reduction of the passive film is less negative at higher phosphate concentration. This behaviour leads one to believe that the species catalyse and stabilize the formation of Fe(II) soluble species during the active dissolution of mild steel and the reduction of the passive film.

The galvanostatic measurements (Fig. 9) suggest that the passive film thickness is almost ten times greater in a phosphate solution than in a bicarbonate one at the same concentration, pH and temperature [1]. If it is assumed that the passive film reduction involves one electron for each iron atom to generate Fe(II) soluble species (by the reaction of Fe(III) + $1e^-$ → Fe(II) involving a reduction charge of 1.3 mC cm^{-2} as a first approximation), it can be deduced that the oxide film after 3 h oxidation at 0.8 V gives a film corresponding to a charge approximately of 4 mC cm^{-2} for its reduction up to $Fe^{(0)}$. The reduction charge is in the same range as the one found in a buffer such as a borate/phosphate mixture [26]. In the latter mixture, the reduction mechanism is possibly a multistep mechanism involving four electrons for the total process [27]. If this mechanism is considered in the case of the present investigation, the charge of the oxide drops to about 2 mC cm^{-2}.

4.3. *Passive film breakdown*

Despite the fact that the nature of the passive film is considered similar in both phosphate and bicarbonate solutions at the same pH, the passive film breakdown induced by the presence of chloride ions shows some differences. The passivity breakdown in bicarbonate occurs at a constant breakdown potential and is characterized by a large upright current increase due to deep pitting (Fig. 12(a)). The solid formed on the surface during the localized attack is

very porous (Fig. 13(a)) and consequently allows solution penetration and displacement of species to and from the pit. Pit growth may continue despite the presence of the corrosion product, that is, without significant inhibition of the corrosion process [2].

In phosphate solutions, the passive film breakdown is manifested first by small current variations, which is characteristic of a breakdown and repair process prior to a large and final current increase (Fig. 12(b)). The presence of a film breakdown prior to its localized repair may be linked to the corrosion product formed on the pits during the localized attack. The SEM picture (Fig. 13(b)) shows the morphology of the precipitate found over the pits. It can be observed that the solid seems less porous for a phosphate solution than for a bicarbonate one and it is deduced that the access of the aggressive anions inside the pit during the localized attack might be more difficult for the former solution. (The dried solid presents some cracks which were probably formed during the drying of the electrode before the surface examination. Such cracks may be generated by drying a cohesive jelly phase.) The formation of some iron-chloride complexes is quite possible on a localized attack site [28–30]. It is reported in the literature that $Fe_3(PO_4)_2.8H_2O$ is obtainable by the reaction between $FeCl_2$ and Na_2HPO_4[17]. Such a reaction may produce the solid covering the pitting sites.

A paper is being prepared on the *in situ* identification of the corrosion products in bicarbonate and phosphate solutions containing chloride ions. The corrosion products is green rust and its chemical composition is related to the composition of the solution.

5. Conclusion

The potentiodynamic curves of 1024 mild steel electrodes in aqueous solutions of various pHs, containing disodium phosphate, display an oxidation peak region at low potentials followed by a passivity region. It is postulated that the rate-determining step in the active dissolution is limited by a diffusion process, most likely an iron/phosphate complex generated during the electrodissolution reaction. The potentiodynamic behaviour of mild steel is more temperature-dependent in phosphate than in bicarbonate solution. The potentiodynamic behaviour in phosphate is also dependent on the composition of the solution and the effects are observed in the active dissolution region and in the reduction of the passive film. The corrosion current related to the localized attack induced by the presence of chloride ions decreases in the phosphate buffer due to the precipitation of a corrosion product.

Acknowledgements

The authors acknowledge the financial support of Hydro-Québec (IREQ), the Natural Sciences and Engineering Research Council of Canada (NSERCC) and the Fonds pour la Formation de Chercheurs et l'Aide à la Recherche (FCAR-Québec).

References

[1] S. Simard, M. Drogowska, L. Brossard and H. Ménard, *J. Appl. Electrochem.* **27** (1997) 317.
[2] S. Simard, L. Brossard and H. Ménard, *J. Appl. Electrochem.* **28** (1998) 151.
[3] G. Gorecki, *Corrosion* **48** (1992) 613.
[4] M. Ogura and M. Kaneko, *Corros. Sci.* **23** (1983) 1229.
[5] N. Sato, T. Noda and K. Kudo, *Electrochim. Acta* **19** (1974) 471.
[6] R. Nishimura and K. Kudo, *Surf. Sci.* **96**, (1980) 413.
[7] K. Ogura and T. Majima, *Electrochim. Acta* **23** (1978) 1361.
[8] K. Ogura, *J. Electroanal. Chem.* **79** (1977) 149.
[9] K. Ogura, A. Fujishima, Y. Nagae and K. Honda, *J. Electroanal. Chem.* **162** (1984) 241.
[10] J. E. O. Mayne and J. W. Menter, *J. Chem. Soc.* (1954) 103.
[11] N. Sato, K. Kudo and T. Noda, *Z. Phys. Chem. Neue Folge* **98** (1975) 271.
[12] K. Tonkunaga, *Jap. J. Appl. Phys.* **21** (1982) 1693.
[13] W. R. Middleton, *Br. Corros. J.* **8** (1973) 62.
[14] K. Azumi, T. Ohtsuka and N. Sato. *J. Electrochem. Soc.* **134** (1987) 1352.
[15] M. J. Prior and M. Cohen, *ibid.* **98** (1951) 263.
[16] Z. Szklarska-Smialowska and R. W. Staehle, *ibid.* **121** (1974) 1393.
[17] C. A. Melendres, N. Camillone III and T. Tipton, *Electrochim. Acta* **34** (1989) 281.
[18] J. G. N. Thomas, *Br. Corros. J.* **5** (1970) 41.
[19] M. Koudelka, J. Sanchez and J. Augustynski, *J. Electrochem. Soc.* **126** (1982) 1186.
[20] R. D. Armstrong, L. Peggs and A. Walsh, *J. Appl. Electrochem.* **24** (1994) 1244.
[21] M. Ergun and A. Y. Turan, *Corros. Sci.* **22** (1991) 1137.
[22] M. Cohen, *Corrosion* **32** (1976) 461.
[23] E. B. Castro, J. R. Vilche and A. J. Arvia. *Corros. Sci.* **32**(1) (1991) 37.
[24] W. J. Albery and M. L. Hitchman. *in* 'Ring-disk Electrodes', Oxford University Press, Ely House, London W1 (1974).
[25] M. E. Brett, K. M. Parkin and M. J. Graham. *J. Electrochem. Soc.* **133** (1986) 2032.
[26] K. Ogura and Y. Miwa, *J. Electroanal. Chem.* **130** (1981) 189.
[27] K. Ogura and K. Sato, *Electrochim. Acta* **25** (1980) 857.
[28] K. E. Heusler and L. Fisher, *Workst. Corros.* **27** (1976) 551.
[29] K. Ogura and M. Kaneko. *Corros. Sci.* **23** (1983) 1229.
[30] S. Kesavan, T. A. Mozhi and B. E. Wilde, *Corrosion* **45** (1989) 213.